An Early Performance Evaluation of the NEXRAD Dual-Polarization Radar Rainfall Estimates for Urban Flood Applications

LUCIANA K. CUNHA

Department of Civil and Environmental Engineering, Princeton University, Princeton, New Jersey, and Willis Research Network, London, United Kingdom

JAMES A. SMITH AND MARY LYNN BAECK

Department of Civil and Environmental Engineering, Princeton University, Princeton, New Jersey

WITOLD F. KRAJEWSKI

IIHR—Hydroscience and Engineering, The University of Iowa, Iowa City, Iowa

(Manuscript received 9 April 2013, in final form 24 July 2013)

ABSTRACT

Dual-polarization radars are expected to provide better rainfall estimates than single-polarization radars because of their ability to characterize hydrometeor type. The goal of this study is to evaluate single- and dual-polarization radar rainfall fields based on two overlapping radars (Kansas City, Missouri, and Topeka, Kansas) and a dense rain gauge network in Kansas City. The study area is located at different distances from the two radars (23–72 km for Kansas City and 104–157 km for Topeka), allowing for the investigation of radar range effects. The temporal and spatial scales of radar rainfall uncertainty based on three significant rainfall events are also examined. It is concluded that the improvements in rainfall estimation achieved by polarimetric radars are not consistent for all events or radars. The nature of the improvement depends fundamentally on range-dependent sampling of the vertical structure of the storms and hydrometeor types. While polarimetric algorithms reduce range effects, they are not able to completely resolve issues associated with range-dependent sampling. Radar rainfall error is demonstrated to decrease as temporal and spatial scales increase. However, errors in the estimation of total storm accumulations based on polarimetric radars remain significant (up to 25%) for scales of approximately 650 km^2.

1. Introduction

Weather radars have been successfully used for many years to monitor rainfall and extreme weather events. In the United States, the first Weather Surveillance Radar-1988 Doppler (WSR-88D) was installed in 1992, and since then 159 single-polarization S-band radars (SPRs) have been deployed. These instruments efficiently detect the structure and evolution of storms and provide quantitative precipitation estimates (QPEs). There are, however, large uncertainties in these QPEs (Wilson and Brandes 1979; Fabry et al. 1992; Baeck and Smith 1998; Smith et al. 1996; Germann et al. 2006; Szturc et al. 2008; Villarini and Krajewski 2009). These uncertainties limit the use of SPR QPEs as input to flood simulation models, especially for urban basins with rapid responses to short-term rainfall rates (e.g., Carpenter and Georgakakos 2004; Javier et al. 2007; Smith et al. 2007; Schröter et al. 2011; Cunha et al. 2012).

One of the major sources of uncertainty in SPR rainfall estimates is the lack of a unique relationship between reflectivity, measured by the radar, and rainfall rate. For SPR QPEs, measurements of reflectivity are converted into rainfall rate (mm h^{-1}) by a power-law relationship ($Z = aR^b$) for which parameters are empirically estimated. Since the parameters of this relationship depend on the raindrop size distribution, which varies between and within storms, there is no unique Z–R relationship that can satisfy all meteorological phenomena. Other factors that lead to inaccuracies in radar-derived rainfall estimates include bright bands (maximums in the radar

Corresponding author address: Luciana Cunha, Department of Civil and Environmental Engineering, Princeton University, E-208, Engineering Quad, Princeton, NJ 08544-0001.
E-mail: lcunha@princeton.edu

DOI: 10.1175/WAF-D-13-00046.1

reflectivity caused by melting snow), incomplete beam filling, calibration errors, attenuation, anomalous propagation (AP), ground clutter, and the sampling strategy used by the radar (e.g., Austin 1987; Fo et al. 1998; Villarini and Krajewski 2009).

Upgrade of the Next Generation Weather Radar (NEXRAD) network to dual-polarization capabilities began in 2011. DPRs have the potential to mitigate some of the uncertainties common to SPRs, since they are able to discriminate between hydrometeors and other aerial targets, and to better characterize the hydrometeor type, as well as the raindrop size distribution illuminated by the radar beam. SPR provides only measurements of horizontal reflectivity, and DPR provides both vertical and horizontal polarization measurements, which are used to estimate differential reflectivity, differential phase shift, and the copolar correlation coefficient [see Straka et al. (2000) for definitions]. These additional variables are used to improve the QPEs. Previous studies have demonstrated the ability of DPRs to classify hydrometeor types (HTs), to identify the melting layer position (Straka et al. 2000; Heinselman and Ryzhkov 2006; Giangrande et al. 2008; Park et al. 2009), and to improve rainfall estimation (Chandrasekar et al. 1990; Ryzhkov et al. 2005b; Vulpiani and Giangrande 2009).

To make the best use of these instruments, we need to fully understand the benefits they provide for QPEs under different meteorological conditions. This is especially true for applications to urban flooding for which high temporal and spatial resolutions, as well as accurate rainfall estimates, are required (Krajewski and Smith 2002; Smith et al. 2002; Einfalt et al. 2004; Wright et al. 2012). In this study we evaluate SPR and operational DPR QPE products collected by the Kansas City, Missouri (KEAX), and Topeka, Kansas (KTWX), radars over the Kansas City metropolitan region. We use Hydro-NEXRAD to estimate SPR QPEs, while DPR QPEs were obtained from the instantaneous precipitation rate (IPR) product of the operational NEXRAD algorithms and provided by the National Oceanic and Atmospheric Administration (NOAA). Both radars overlap an area with a very dense network of rain gauges. Our goal is to better understand QPE improvements achieved by DPRs, and how they can improve flood prediction across multiple scales.

We present an error analysis of QPEs by comparing the different radar rainfall products with rain gauge data. We evaluate possible causes of errors in SPR and DPR QPEs and assess how QPE uncertainties vary across a range of temporal and spatial scales. Our focus is on urban flooding, and our evaluation is for basins with drainage areas varying from approximately 1 to 650 km^2 in the Kansas City area.

This works centers on the following questions: Are rainfall estimates based on DPRs (consistently) better than rainfall estimates based on SPRs? If not, in which situations are they better or worse? What is the effect of range on radar rainfall estimation based on DPRs and SPRs? Do DPRs provide better estimates of hydrologically relevant rainfall properties that lead to improved prediction of flash floods?

In the following section, we present the study area and experimental data. In section 3, we present the analysis methods applied in this study. In section 4, we examine the main results; and in section 5, we discuss our conclusions and recommendations for future research.

2. Study area, data, and methods

In this study we compare rainfall fields obtained by SPRs and DPRs with ground reference data obtained from a dense rain gauge network in the Kansas City metropolitan area. We analyze radar rainfall estimates for three rainfall events that occurred on 19–20 March 2012, 6–7 May 2012, and 31 August–1 September 2012. Each of the storms occurred after the implementation of the DPR upgrades to the KEAX (10 February 2012) and KTWX (30 January 2012) WSR-88Ds. The three storms exhibited very different characteristics in terms of the spatial variability of rainfall over the study region, the magnitudes of the rainfall rate, and the distribution of hydrometeor types. We will describe these differences in the results session.

a. Rain gauge network

The city of Overland Park and Johnson County, Kansas, maintain a dense rain gauge network with the goal of mitigating urban floods. The network collects rainfall data in near–real time with high temporal resolution (less than 5 min) and makes the data freely available (www.stormwatch.com). The network includes 136 tipping-bucket rain gauges that were operational for the year 2012; most of the gauges are High Sierra model 2400 gauges (M. Ross 2012, personal communication). The bucket volume is 1 mm and the collected data are transmitted to the base server in near–real time. While the bucket size is too coarse for detailed studies of rainfall rate variability (see Habib et al. 2001), it is deemed adequate for high-intensity and accumulation events that produce flash floods.

We collected raw data in breakpoint format (times of 1-mm tips) and estimated 15-min rain rates using the tip interpolation method. Ciach (2003) demonstrated the advantage of the tip interpolation method compared to the traditional tip-counting method, especially for shorter time scales. Even though we use gauge-based

estimates as ground reference, we recognize that tipping-bucket rain gauge data are subject to systematic and random instrumental errors (Zawadzki 1975; Austin 1987; Habib et al. 2001; Lanza and Stagi 2008).

The accuracy of the gauge versus radar comparisons is limited by the space–time sampling differences of both instruments. While tipping buckets sample areas on the order of $10^{-1}\,m^2$, radar samples areas of approximately $1 \times 10^6\,m^2$. The severity of the effect depends on the spatial variability of rainfall at a given temporal scale. Due to the small sample of storms available for this study, we did not pursue the error variance and covariance separation method (Ciach and Krajewski 1999; Mandapaka et al. 2009) that ''isolate'' errors due to sampling scale differences. Nevertheless, the radar versus gauge comparison does provide diagnostic information pertinent to our goal of comparing SPR and DPR precipitation estimates. The scale problem is especially relevant in the comparison of 15-min gauge and radar rain rates, but it is minimized as we aggregate the observations in space or time (Ciach and Krajewski 1999; Seo and Krajewski 2010; Seo and Krajewski 2011). We examine both storm total analyses (aggregation in time) and basin-scale error analyses (aggregation in space).

b. Radar rainfall data

In this study we developed SPR and DPR rainfall fields over an area of approximately $3600\,km^2$ (60 km by 60 km centered) around Kansas City, using observations from both the KEAX and KTBW radars. The distance from the KEAX radar to the rain gauges in the Kansas City network ranges from 23 to 72 km, while the distance from the KTWX radar ranges from 104 to 157 km. The difference in distance from both radars to the study area allows us to investigate the effects of range on QPE uncertainty. Range effects on radar rainfall estimation were previously demonstrated by Smith et al. (1996), Fo et al. (1998), Fulton et al. (1998), and Krajewski et al. (2011b).

Figure 1a shows the locations of the two radars and their distances to the study area, Fig. 1b presents a map with the rain gauge locations, and Fig. 1c illustrates a vertical profile where we indicate the radar beam geometry and height over the study area for both radars for the lowest elevation angle. Range effects are caused mainly by an increase in the radar beam height and radar echo vertical structure heterogeneity with range. Depending on the range, the radar beam might partly intercept the melting layer or even completely overshoot precipitation.

For both radars we will compare rainfall fields that are based on the SPR-only and DPR NEXRAD measurements. Herein, we refer to KEAX-SPR and KTWX-SPR for single-polarization (conventional NEXRAD system) data and KEAX-DPR and KTWX-DPR for dual-polarimetric data.

For the generation of the 15-min SPR NEXRAD rainfall fields we collected level II data from the National Climatic Data Center (NCDC) for the two radars. We used the Hydro-NEXRAD radar-rainfall estimation algorithms to convert reflectivity into 15-min rainfall accumulation fields at 1-km horizontal resolution. Hydro-NEXRAD capabilities and the procedures used to generate rainfall products are described in Krajewski et al. (2011a) and Krajewski et al. (2007). The preprocessing rain-rate algorithm converts reflectivity from the lowest elevation angle scan to rainfall rate using the standard Z–R relationship for convective events (Fulton et al. 1998). The user can specify the power-law empirical relationship between the reflectivity and rainfall intensity. For this study we applied the ''quick look'' algorithm (refer to Krajewski et al. 2011a), which provides standard parameters ($Z = 300R^{1.4}$) to generate 15-min and 1 km $\times$ 1 km accumulated rainfall maps. We applied a quality control algorithm that performs anomalous propagation correction (Steiner and Smith 2002), but omits range correction and advection correction. Hydro-NEXRAD provides rainfall fields with a nominal grid resolution of 1 km $\times$ 1 km in the Super Hydrologic Rainfall Analysis Project (SHRAP) format based on the HRAP algorithm of Reed and Maidment (1999). We used standard procedures to reproject the dataset to geographic coordinates.

In this study, we utilized the operational instantaneous precipitation rate (IPR) product to derive the DPR rainfall fields for both KEAX and KTBW. The DPR rainfall algorithms (Istok et al. 2009) were developed in part from the results obtained by the Joint Polarization Experiment (JPOLE) described by Ryzhkov et al. (2005b), Heinselman and Ryzhkov (2006), and Park et al. (2009).

One of the advantages of DPR is the classification of the hydrometeor type in the sample volume. In addition to the IPR rainfall fields, we also use the operational hybrid hydrometeor classification (HHC) fields. For the initial operational capabilities the NEXRAD agencies defined the following hydrometeor classes: 1) biological, 2) ground clutter and anomalous propagation, 3) ice crystal, 4) dry snow, 5) wet snow, 6) light–moderate rain, 7) heavy rain, 8) big drops, 9) graupel, 10) hail (mixed with rain), and 11) unknown. The HTs are defined based on a fuzzy logic method that takes into consideration measurement uncertainties: lower weights are given to uncertain measurements in the classification scheme. The melting layer (ML) position is usually identified based on the layer with maximum reflectivity and differential

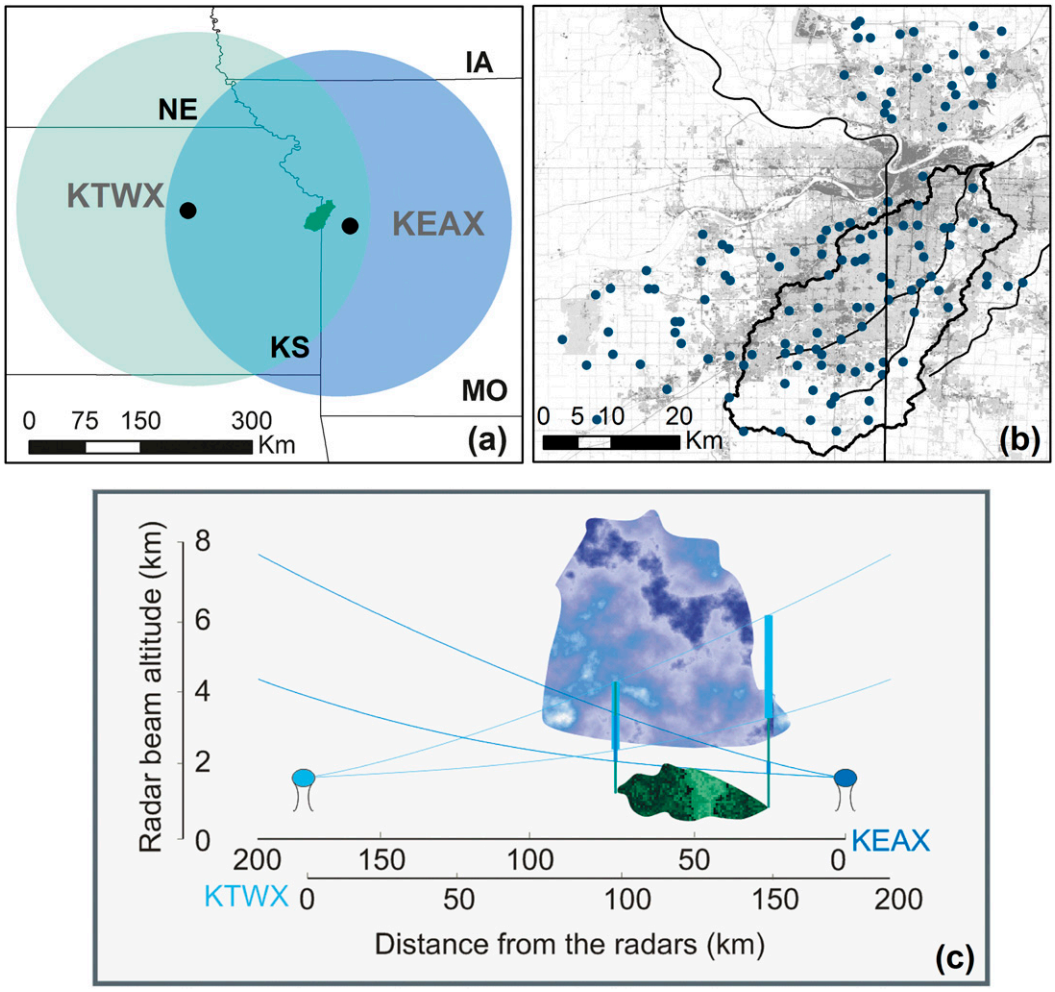

FIG. 1. (a) The 200-km umbrellas of the KEAX and KTWX radars and the basin location. (b) Rain gauge locations (blue dots) with gray shading denoting different degrees of the Kansas City impervious area (2006). (c) A schematic vertical profile where the KEAX and KTWX sampling areas (beam geometry and height) above the basin are indicated.

reflectivity, and minimum correlation coefficient (Brandes and Ikeda 2004; Giangrande et al. 2008). Based on these parameters a snow score is estimated and used to define the melting-layer top and bottom. When the melting layer cannot be identified by this procedure, the top of the melting layer is defined at the 0°C isotherm and the bottom is located 500 m below the top. The 0°C isotherm is obtained from the Rapid Update Cycle model [see Benjamin (1989) and Schuur et al. (2011) for details]. Once the height of the melting layer is defined, the HHC is estimated based on the best–lowest available scan for each location. The HHC and the melting layer position determine the rainfall-rate estimation algorithm (Giangrande and Ryzhkov 2008). Note that the different procedures used to define the melting layer can be a source of uncertainty on the definition of HHC and consequently on QPE estimation.

Table 1 presents a summary of the hydrometeor classes and estimation equations used. These equations are defined by Giangrande and Ryzhkov (2008) based on empirical data for Oklahoma. They note that the parameters for these equations are optimized for the Oklahoma data and that the validity of the equations should be tested using data collected under different climatological conditions.

Differential reflectivity Zdr and reflectivity Z are used in the case of light, moderate, and heavy rain, and big drops. In the case of hail below the melting layer, only DZ is used. For the remaining cases (wet snow, graupel, hail above the melting layer, dry snow, and ice crystals), the standard Z–R relationship is used and a fixed correction is performed depending on the class (Ryzhkov et al. 2005b). For example, for wet snow the value calculated by the standard Z–R relationship is

TABLE 1. Hydrometeor types and radar rainfall estimation equations.

Symbol	Hydrometeor type	Position in relation to the ML*	Rain equation
GC	Ground clutter–anomalous propagation	CB, PB, PA, MW	$R = 0$
BI	Biological	CB, PB, MW, PA	$R = 0$
RA	Light–moderate rain	CB or PB	$R(Z, \mathrm{Zdr})$
HR	Heavy rain	CB or PB	$R(Z, \mathrm{Zdr})$
BD	Big drops	CB, PB, MW, PA	$R(Z, \mathrm{Zdr})$
HA	Hail mixed with rain	CB, PB, MW, PA	$R(\mathrm{Zdr})$
		CA	$0.8R(Z)$
DS	Dry snow	CB, PB, MW, PA	$R(Z)$
		CA	$2.8R(Z)$
WS	Wet snow	PB, MW, PA	$0.6R(Z)$
GR	Graupel	PB, MW, PA, CA	$0.8R(Z)$
IC	Ice crystal	CA	$2.8R(Z)$
UK	Unknown	All	$R(Z)$

* CB = completely below, PB = partly below, MW = mostly within, PA = partly above, and CA = completely above.

reduced by 40%, and for graupel and hail by 20%. For dry snow and ice crystals, the Z–R values area increased by 280%.

Some of the HHC classes are identified only if the radar beam partly (or completely) overshoots the rainfall and intercepts parts of the melting layer. For example, ice crystals are observed if the radar beam completely overshoots the melting layer. Graupel, dry snow, and wet snow are typically all present when part of the radar beam is actually sampling the melting layer. We use these classes to identify the regions in the study area for which either the KEAX or KTWX radar overshoots the rainfall. Overshooting is more likely to happen for KTWX since it is located farther from the study area.

The IPR fields are in a polar coordinate system and we used the NOAA toolkit to transform the data to geographical coordinates, with spatial resolution of approximately 1 km × 1 km. Both IPR and HHC fields are provided for each volume scan. In the typical rainfall mode operation, NEXRAD radars collect a volume scan every 4–6 min. To obtain 15-min time series, we first interpolated both variables to produce maps with 1-min time resolution. We then aggregate the 1-min values to the desired temporal resolution (15, 30, and 60 min). For IPC, we applied linear interpolation, while for HHC we used the nearest-neighbor interpolation method.

c. Methods

The goal of this paper is to assess improvements in QPEs obtained by dual-polarization radars and to explore the potential of applying this dataset to urban hydrology even when ground data are not available. Therefore, we evaluate radar rainfall estimates without removing systematic biases relative to rain gauges. Moreover, this correction requires long series of data, which are not yet available for polarimetric radars. For all the analyses performed in this paper, we calculate the normalized bias (NB); the standard error (SE), also called root-mean-square error; and the Pearson correlation coefficient (CORR), which are defined as follows:

normalized bias,

$$\mathrm{NB}_{(s)} = \frac{\sum D_{(s,t)} - \mathrm{Dref}_{(s,t)}}{\sum \mathrm{Dref}_{(s,t)}};$$

standard error,

$$\mathrm{SE}_{(s)} = \sqrt{\frac{\sum [D_{(s,t)} - \mathrm{Dref}_{(s,t)}]^2}{N}}; \quad \text{and}$$

Pearson correlation coefficient,

$$\mathrm{CORR}_{(s)} = \frac{\mathrm{cov}[D_{(s,t)}, \mathrm{Dref}_{(s,t)}]}{\sigma_{D(s)} \times \sigma_{\mathrm{Dref}(s)}}$$

$$= \frac{E[D_{(s,t)} - E[D_{(s,t)}]] \times E[\mathrm{Dref}_{(s,t)} - E[\mathrm{Dref}_{(s,t)}]]}{\sigma_{D(s)} \times \sigma_{\mathrm{Dref}(s)}}.$$

CORR measures the degree of linear association between the radar and gauge measurements. The quantities $E[X]$ and σ_X are the expected value and the standard deviation of X, respectively. NB and CORR are dimensionless, and SE is in millimeters or millimeters per hour. The index s refers to a specific spatial domain that can be a gauge location or a subbasins, and t to the time intervals. NB is a measure of the overall bias (B), which represents systematic average deviations of radar estimates with respect to the rain gauge estimation over the spatial domain of interest (gauge location or subbasin). SE is a measure of dispersion and indicates how

radar measurements differ from their expected value (gauge estimation). Since we do not remove the mean field bias, SE accounts for systematic and random errors. CORR measures the degree of linear association between the radar and gauge measurements.

Depending on the analyses, the variables D and Dref represent total storm accumulations (mm) or 15-min rain-rate values (mm h^{-1}) calculated based on different rainfall datasets (gauge, SPR, or DPR) estimated over a point/pixel or over a certain spatial domain (subbasin). The Dref refers to the gauge data, and the D to one of the radar products. For the point analyses, the summations refers to each ith radar–gauge pair, yielding a sample size by event equal to the number of sites for total storm accumulations, and the number of sites times the number of 15-min intervals for the rain-rate comparisons.

Rainfall is the main input for many hydrological models; therefore, it is important to understand how rainfall errors change across scales to be able to decide if a certain dataset is adequate for hydrological application (from hillslope to large-scale hydrology), and to better understand uncertainties on the results of the hydrological models (Seo et al. 2013). Previous studies have demonstrated that radar rainfall estimation errors decrease with averaging in space and time (e.g., Knox and Anagnostou 2009; Seo and Krajewski 2010). This is expected since averaging a large number of observations reduces random uncertainties. This is relevant for the hydrological community, since it means that even if errors are large for small scales (e.g., 15 min in time, 1 km × 1 km in space), there should be a scale for which errors are in an acceptable range for flood applications.

In this study, we aggregate the information in time (15–180 min) and in space (0.02–650 km^2) and calculate statistical measures described in the previous sections (NB, SD, and CORR). Because our focus is on providing information about radar rainfall error scaling in a hydrologic context, we aggregate the information in space using basin boundaries, which are natural spatial domains in hydrology. We use the river networks analysis tool CUENCAS [see description in Mantilla and Gupta (2005) and Cunha et al. (2011)] to automatically extract the river network and the basin boundaries based on the U.S. Geological Survey's (USGS) National Elevation Dataset (NED) 30-m Digital Elevation Map (DEM; Gesch et al. 2009). We interpolate 15-min rain gauge data using the inverse-distance-weighting method to generate spatially continuous rainfall maps with the same resolution as the radar maps. The interpolated datasets are used as reference to evaluate radar rainfall estimates. Due to the high density of gauges (see Fig. 1b), the interpolated maps provide accurate representation of the rainfall spatial variability in the basin. We calculate statistical measures and hydrologic parameters that are relevant for flood simulation, including mean areal accumulated rainfall and mean areal maximum rainfall intensity, for each of the nested subbasins, ranging in scale from 0.01 to 650 km^2. We estimate the mean areal rainfall for each basin based on the weighted average of all radar pixels that are enclosed or intersected by the basin. The weight is proportional to the area of the pixel that is contained by the basin. Note that even very small basins can partially intersect more than one pixel.

3. Results

a. Flood summary and storm totals

The March, May, and September 2012 storm events exhibit contrasting characteristics in terms of rainfall distribution over the study region, magnitudes of rainfall rate, melting-layer position, and HT. In Fig. 2, we illustrate the spatial structure of the storm total radar rainfall for a 160 km × 120 km domain that contains the Kansas City study region.

The 6–7 May 2012 storm (Fig. 2) was an organized thunderstorm system that produced damaging winds and hail. The storm total rainfall fields exhibit large spatial variability associated with the structure and evolution of the storm system. In Fig. 2, we present rainfall fields derived from both the DPR and SPR algorithms for both the KEAX and KTWX radars. In addition to the spatial variability in storm total rainfall for each of the four rainfall fields, there are also striking contrasts among the four radar rainfall fields. One of the central questions we want to address is whether the DPR rainfall estimates are superior to the SPR rainfall estimates. Over the Kansas City study region, rain gauge storm totals varied from 10 to 130 mm and peak rainfall intensities reached 150 mm h^{-1} at 15-min time resolution. During this event, the U.S. National Weather Service issued numerous flood warnings for Johnson, Jackson, and Cass Counties that covered the Kansas City area. The local news channel (KSHB, channel 41) reported the occurrence of 1-in. hail in the southeast part of the city.

The 19–20 March 2012 storm was a typical spring extratropical system that produced moderately heavy rainfall (Fig. 3a) over time periods of 12–24 h. Over the course of the event there was a temperature drop of approximately 12°C (21°–9°C) as a cold front passed through the region; the melting layer was low over the entire duration of the storm. The KEAX radar detected a few periods (approximately 1% of the time, for selected regions) with dry snow, while the measurements performed by the KTWX radar included ice crystals, dry snow, wet snow, and graupel. These are hydrometeor

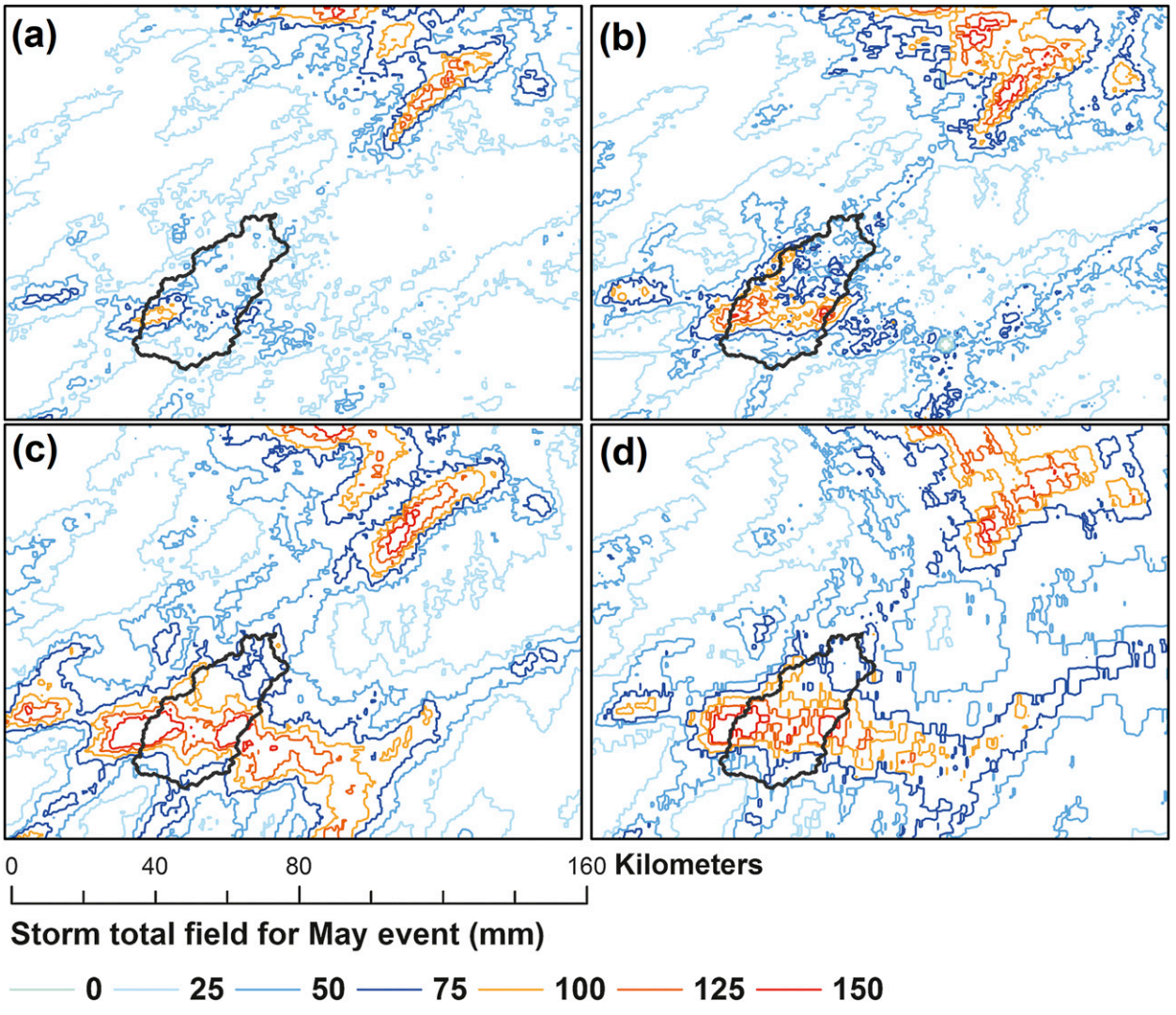

FIG. 2. Storm total accumulation field (mm) derived from (a) KEAX-SPR, (b) KEAX-DPR, (c) KTWX-SPR, and (d) KTWX-DPR for the May 2012 storm.

types observed only in the melting layer. The storm total measured by rain gauges varied from 45 to 70 mm over the Kansas City study area.

The 31 August–1 September storm is typical of fall extratropical systems that produce high storm total rainfall (Fig. 3b) over time periods of 12–24 h. The storm period was characterized by a cold front that became stationary over the region. In the beginning of the period, temperatures dropped from a maximum of 38°C to 18°C and then remained constant for the rest of the period. The event was characterized by low-intensity rainfall that lasted a long period, resulting in storm totals that varied from 76 to 222 mm over the Kansas City study area.

In Fig. 4, we present maps of hydrometeor-type frequency for the KTWX radar for all events. The maps represent the percentage of the time for which the radar classified the radar target as ice crystal, dry snow, wet snow, or graupel during each storm. For the March event among the hydrometeor types are ice crystals, implying that the radar beam overshoots the precipitation. Dry snow, wet snow, and graupel are identified when the radar beam is observing the melting layer. For the March and May events, the melting layer affects rainfall estimates. For the September event there is only a brief period of time for which the bright band affects the rainfall estimates.

In Fig. 5, we present the frequency of HT for the May event, for light–moderate rain, heavy rain, big drops, and hail for the KEAX and KTWX radars. The maps would be identical if both radars were observing the same layer of the atmosphere and if the HT classification procedure was error free. The HT observed indicated that the radar beam captures at least part of the atmosphere

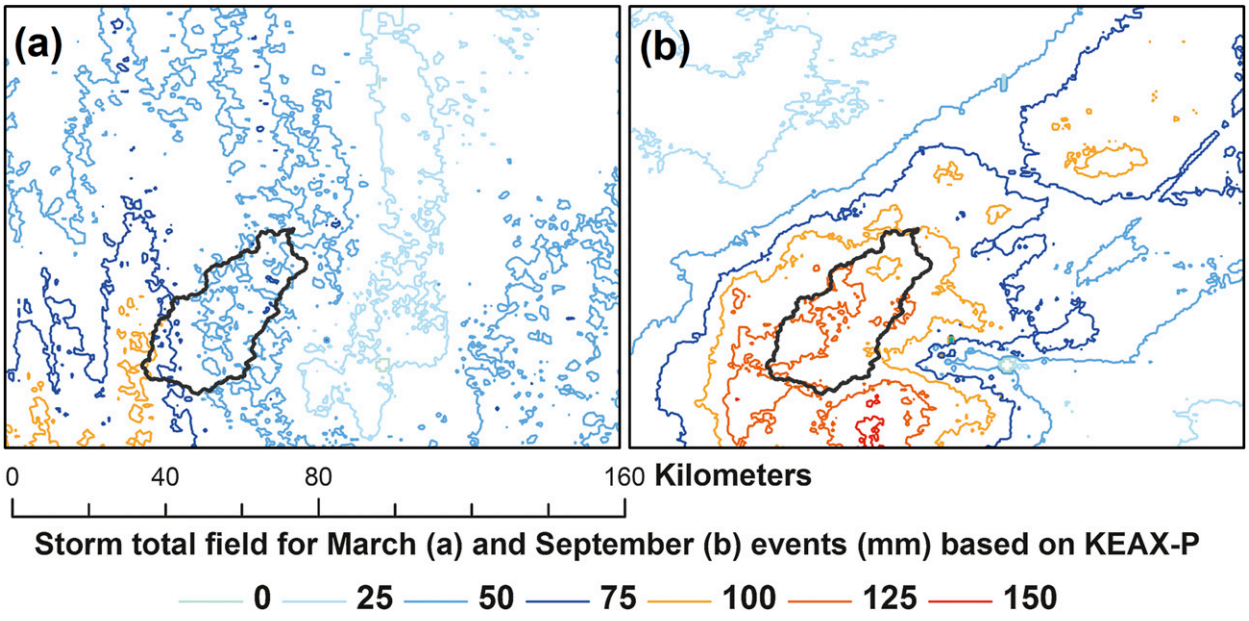

FIG. 3. Storm total accumulation field (mm) derived from KEAX-DPR for the (a) March and (b) September 2012 storms.

below the melting layer. There are several reports of hail on the ground during the May event. Both radars detected hail mainly in the southern part of the study region. The KTWX radar observed much more hail and more big drops than did the KEAX radar. This is expected because the KTWX radar is sampling higher layers of the atmosphere. KEAX detected more heavy rain in the same areas where KTWX detected more hail.

Figure 6 presents gauge versus radar scatterplots of storm total rainfall values for the March (green), May (blue), and September (red) events for SPR (top) and DPR (bottom) rainfall estimates and for the KEAX (left) and KTWX (right) radars. Table 2 summarizes the normalized bias, standard errors, and correlation of storm total radar rainfall estimates using rain gauge observations as reference data. We also include the average (of all gauges) of the percentage of time that each hydrometeor type was identified by KEAX and KTWX. The values are calculated for each event and for all the events together. Note that the KEAX-SPR always underestimates the storm totals for the March and September events, and almost always for the May event. Close-range biases for SPR are likely caused by a biased Z–R relationship that compensates for the typical brightband contamination (Smith et al. 1996); the absence of brightband contamination in this case leads to underestimation at close range. For the May event, KEAX-SPR overestimates storm totals for some of the gauges. Overestimation occurs for gauges with very low storm totals in the southwest and in the north of the basin (less than 20 mm) and for regions where hail was detected. The KEAX-DPR rainfall estimates do not exhibit systematic underestimation of storm totals. Although smaller in magnitude, bias still exists for the DPR rainfall estimates. For the March and May storms, the normalized bias shifts signs from SPRs to DPRs. KEAX-DPR overestimates the storm total accumulations. For the September storm, both KTWX-SPR and KEAX-DPR underestimate the storm total but KEAX-DPR has a smaller normalized bias.

KTWX-SPR also underestimates the storm total rainfall for the September event, for which no brightband contamination occurs even at the far ranges. It is likely that even at these far ranges the effect of biased Z–R relationships can be seen when no brightband contamination occurs. The opposite effect occurs for the events with brightband contamination, for which KTWX-SPR overestimates rainfall. The absence of a systematic pattern in normalized bias will be discussed in the next section where we elaborate upon range effects on storm totals.

The correlation between storm total rainfall from radar and rain gauge storm total accumulations is larger for all three events for the KEAX radar (Table 2). For the KTWX radar, DPR rainfall estimates have a larger correlation than SPR rainfall estimates for the May and September storms, but not for the March storm. The normalized bias is closer to 0 for the May and September events for KEAX-DPR rainfall estimates. For KTWX-DPR, the normalized bias is closer to 0 for the May storm, but not for the March and September events.

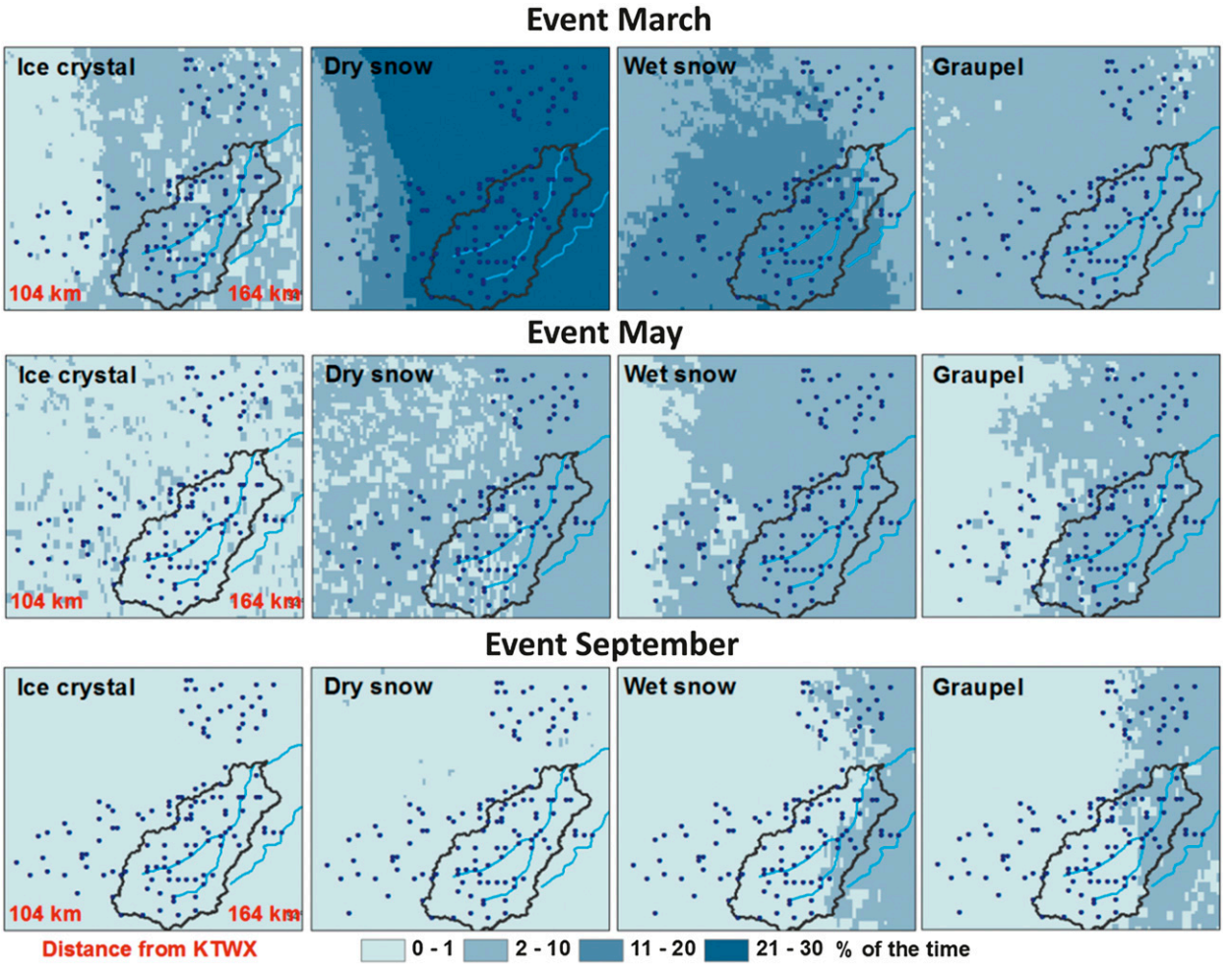

FIG. 4. Frequency of (from left to right) hybrid hydrometeor classification for KTWX for HTs typical of the melting layer: (from top to bottom) March, May, and September. These hydrometeors are not identified by the KEAX radar since it is located very close to the study area and the radar beam is always below the melting layer.

These features are closely linked to range-dependent sampling of the radars, as detailed below.

b. *Range effects on storm totals*

Figure 7 presents the normalized bias for storm total rainfall versus radar range for the KEAX (ranges up to 72 km) and KTWX (ranges larger than 104 km) for SPRs (blue) and DPRs (red) for the March, May, and September events. Each point represents NB values for a rain gauge location. We also include the moving-average lines estimated with a 10-km window to facilitate visual evaluation of the data (blue and red lines). This representation of range-dependent bias reflects some of the issues discussed in the previous section, but also provides information about how radar uncertainties and improvements from SPR to DPR rainfall estimates vary with range.

KEAX storm total accumulations estimated by the DPRs are always higher than the rainfall estimates by SPRs. As previously noted, SPRs use the traditional Z–R relationship and the parameters of this relationship cannot account for range-dependent effects of brightband contamination. For the DPRs, rainfall is estimated based on reflectivity, differential reflectivity, and hydrometeor class. The estimation algorithm generally results in lower bias; however, for the March event, KEAX-DPR overestimates storm totals relative to rain gauges. For the September event, KEAX-DPR underestimates the storm total in relation to the gauges. For the May event we observe a large degree of scatter, likely resulting in part from the large variability of HT and storm totals as indicated by Figs. 2 and 5, respectively. Independent of the scatter, the regression lines show that the differences between KEAX-SPR and KEAX-DPR follow the same tendency as the ones observed for the other events.

For the KTWX radar the changes between the DPR and SPR rainfall estimates are not always consistent. For

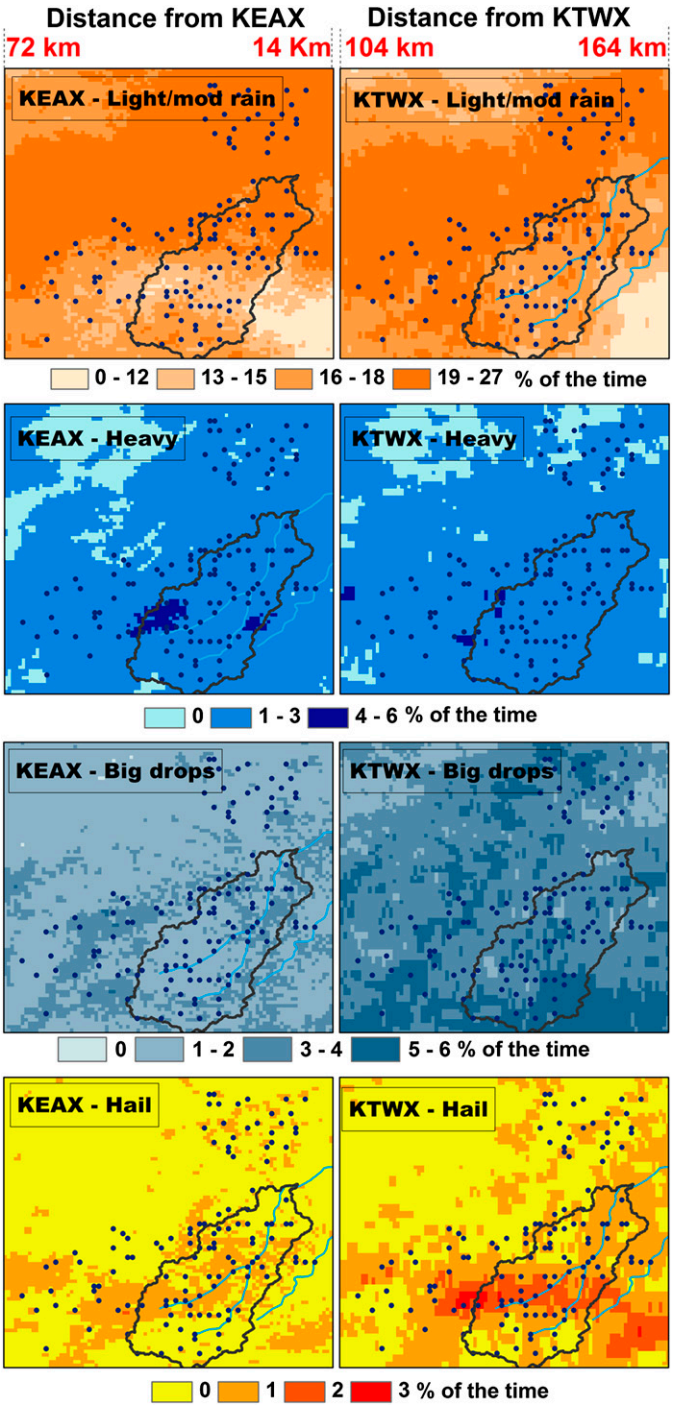

FIG. 5. Frequency of hybrid hydrometeor classification for (left) KEAX and (right) KTWX for the May event: (from top to bottom) light–moderate rain, heavy rain, big drop rain, and hail.

the September event, we observe almost no difference between the KTWX-SPR and KTWX-DPR storm totals. For the March event, the differences between KTWX-SPR and KTWX-DPR are large. KTWX-DPR improved storm total estimates for ranges up to approximately 130 km but the estimates deteriorated at larger ranges. For the May storm, we observed significant changes between KTWX-DPR and KTWX-SPR for ranges up to 125 km, some

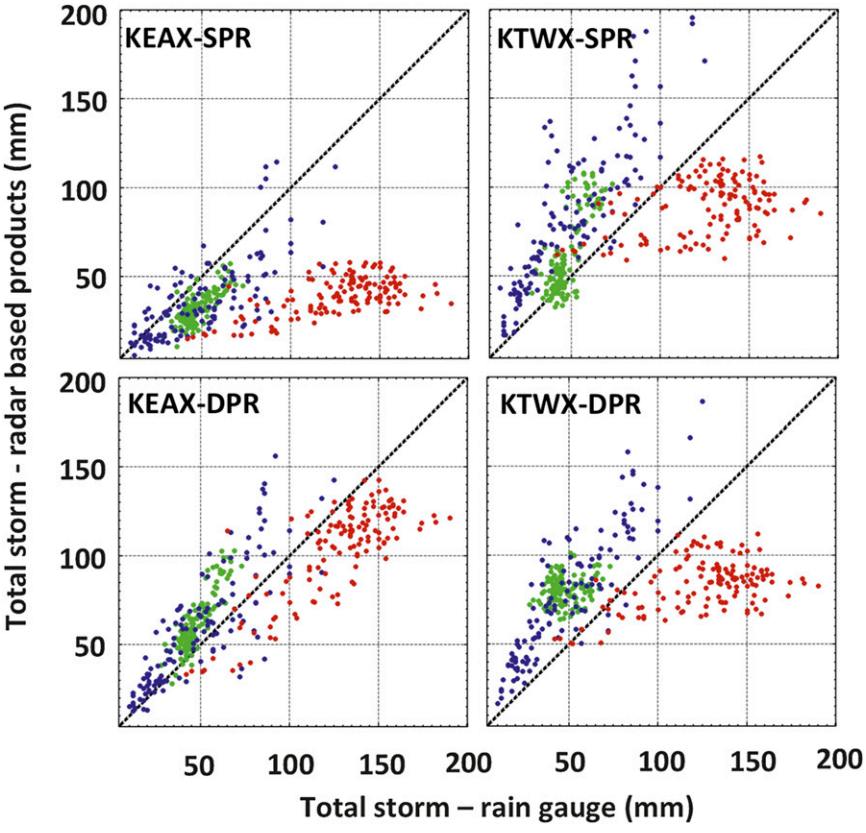

FIG. 6. Scatterplot of gauge vs radar rainfall accumulation for the March (green), May (blue), and September (red) events for the (top) SPR and (bottom) DPR datasets and for (left) KEAX and (right) KTWX.

changes in the 125–140-km range, and almost no changes for ranges larger than 140 km.

Based on HHC frequency for the May and September storms (Table 2), the percentage of light–moderate rain is not significantly different between KTWX and KEAX. The main difference is that KTWX detects periods with graupel, dry snow, wet snow, and ice crystals—hydrometeors typical of the melting layer—while KEAX does not detect these HTs. Moreover, KTWX detects hail more frequently than KEAX. For the March event, significant differences are observed between the hydrometeor frequency observed by KEAX and by KTWX. For that event, KTWX almost always samples above the melting layer, resulting in large errors for KTWX-DPR rainfall fields. We will discuss this issue in the following section.

c. Gauge–radar 15-min rain-rate intercomparison

In the previous section we showed that differences between storm total accumulation based on KTWX-SPR and KTWX-DPR for the March event are not always consistent and are range dependent. We observe two opposing patterns of behavior: for ranges less than 125 km, KTWX-DPR exhibits superior estimation of storm total rainfall compared to KTWX-SPR, and for ranges greater than 125 km, KTWX-DPR storm total rainfall estimates are worse than those of KTWX-SPR. In this section, we use the 15-min rain-rate fields and the hydrometeor frequency time series to investigate the cause of these contrasts.

In Figs. 8 and 9, we analyze the time series of rain rate (gauge, SPR, and DPR) and HT frequency of two gauges, located at distances of 105 km (gauge 1) and 152 km (gauge 2) from KTWX and 69 km (gauge 1) and 47 km (gauge 2) from KEAX. Figures 8 and 9 present the 15-min rain-rate time series from the rain gauges, KTWX-SPR, KEAX-DPR, KTWX-SPR, and KTWX-DPR, as well as the HT frequencies for KEAX and KTWX. These two examples demonstrate the lack of consistency in improvements obtained by DPRs. For gauge 1 (Fig. 8), KEAX overestimates the first rainfall peak for both the DPRs and SPRs, with the DPR estimate being worse than that for the SPRs. For KTWX, the DPRs overestimate and SPRs underestimate the same peak, with the DPR estimation being considerably

TABLE 2. Storm total statistics for all rainfall datasets and events.

		Mar	May	Sep	All
Gauge	Avg (mm)	47.40	49.59	126.77	
	Std dev (mm)	8.75	26.95	30.13	
	Coefficient of variation	0.18	0.54	0.24	
NB	KTWX-SPR	−0.31	−0.26	−0.69	−0.52
	KEAX-DPR	0.31	0.21	−0.19	0.00
	KTWX-SPR	0.29	0.69	−0.30	0.04
	KTWX-DPR	0.70	0.56	−0.34	0.07
CORR	KTWX-SPR	0.77	0.73	0.61	0.46
	KEAX-DPR	0.87	0.83	0.81	0.86
	KTWX-SPR	0.77	0.85	0.38	0.53
	KTWX-DPR	0.22	0.89	0.48	0.43
SE	KTWX-SPR	15.95	22.55	91.02	55.39
	KEAX-DPR	17.28	21.13	29.65	23.32
	KTWX-SPR	21.24	41.18	46.86	38.02
	KTWX-DPR	34.87	32.48	50.51	40.23
KEAX HT avg frequency	% RA	28.87%	18.69%	54.88%	34.14%
	% HR	0.32%	1.10%	0.00%	0.47%
	% BD	0.29%	1.67%	0.21%	0.72%
	HA	0.01	0.07	0.00	0.03
	% GR, DS, WS, and IC	0.04%	0.00%	0.00%	0.01%
	% others; no rain	70.47%	78.47%	44.91%	64.62%
KTWX HT avg frequency	% RA	5.05%	17.58%	54.85%	25.83%
	% HR	0.08%	1.09%	0.00%	0.39%
	% BD	0.31%	1.70%	0.22%	0.74%
	HA	0.05	0.34	0.00	0.13
	% GR, DS, WS, and IC	41.98%	6.30%	0.72%	16.33%
	% others; no rain	52.52%	73.00%	44.20%	56.57%

better than that of the SPRs. For the remaining time period, with lighter rain, the KTWX-DPR and KTWX-SPR rainfall estimates are similar for this gauge. For gauge 2 (Fig. 9), KEAX-DPR provides a better estimation of the peak than KEAX-SPR, while the KTWX-SPR and KTWX-DPR estimates of the first peak are practically the same. However, KTWX-DPR and KTWX-SPR provide distinct rainfall estimates for the period with light rainfall. KTWX-SPR did not identify rainfall for many periods, while KTWX-DPR overestimated rain. Note that KEAX observes mainly (almost 100%) hydrometeors associated with rain (RA + HR + BD) for both gauges, while KTWX observes a mix of rainfall and melting layer HTs. When analyzing Figs. 8 and 9, we should remember that tipping-bucket errors are large for low-intensity rainfall and that this instrument fails to identify the time that the rainfall started and ended. Nevertheless, the volume of rainfall should be similar, which is the case for the gauge 1 estimates at KTWX and KEAX, but not for gauge 2, with KTWX-DPR overestimating and KTWX-SPR underestimating the rainfall. The difference in bias among the KTWX DPRs and SPRs for gauge 2 occurs because the DPR algorithm overcorrects rain rates for frozen hydrometeors, while the standard Z–R relationship underestimates rain rates when applied for these hydrometeors.

Analyses of 15-min rainfall rates (Fig. 10) indicate that the DPR rainfall estimates for KEAX are significantly better than the SPR rainfall estimates in terms of both bias and standard error. Figure 10 presents a scatterplot of 15-min rain gauge rainfall rate versus 15-min radar rainfall rate for the radar bin containing the gauge. The points are color coded by event: green for the March event, blue for the May event, and red for the September event. We use power-law functions to describe the differences between radar and gauge rainfall as a function of rain rate (deterministic error) (Ciach et al. 2007; Villarini et al. 2009). We estimate the parameters of the power-law function for each rainfall product and event using the Levenberg–Marquardt algorithm. The improvement in the 15-min radar rainfall estimates for KEAX-DPR from KTWX-SPR is clear, while KTWX-SPR and KTWX-DPR show very similar rain-rate estimates.

In Table 3, we summarize the 15-min rainfall estimation properties for KEAX and KTWX and for SPR and DPR measurements. To remove the effects of very low values (for which gauges are not very accurate), we calculate CORR, NB, and SE based on the periods for which gauges observed 15-min rain rates larger than $4\,\text{mm}\,\text{h}^{-1}$. The correlation improves from SPRs to DPRs for all events and both radars, except the May storm for KTWX. For the March storm, NB and SE are

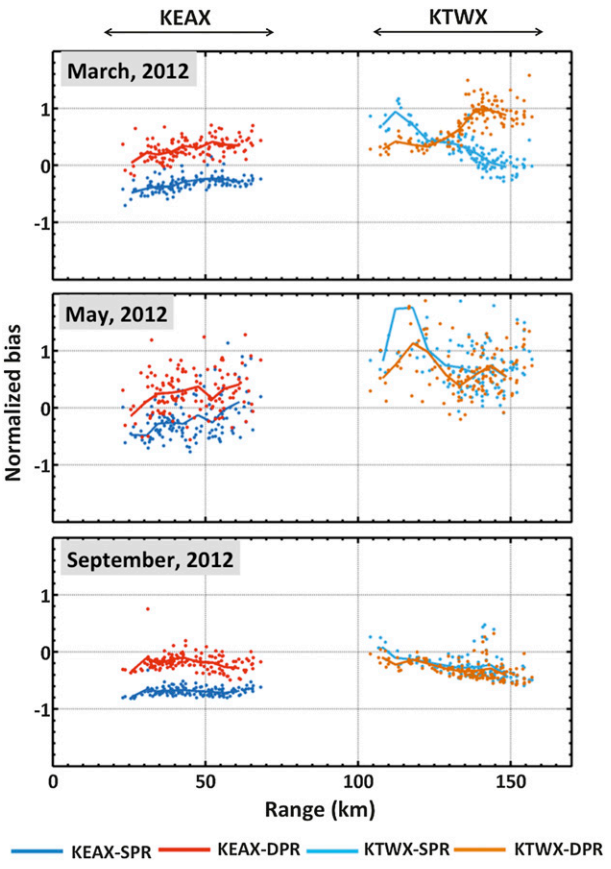

FIG. 7. Normalized bias as a function of range for the (top) March, (middle) May, and (bottom) September events and for SPR (blue) and DPR data (red). Ranges up to 70 km correspond to KEAX and ranges larger than 100 km to KTWX.

considerably higher for the KEAX DPRs than for the SPRs (from 0.50 to −0.28 for NB and from 9.42 to 5.75 for SE; green dots in Fig. 6). For the May and September events, KEAX-DPR performs better than KTWX-SPR. One important point to note is the reduction of spread that is probably the result of including HTs in the rainfall estimation algorithm. For the KTWX radar, changes from SPR to DPR are not substantial for the May and September events. Because we focus on large rain-rate values, for the March event, the DPRs provide better measurements than do the SPRs. For all cases the DPRs provide better estimates of maximum rainfall than do the SPRs, with the exception of the KEAX March event for which the maximum rainfall was overestimated by 58%.

To understand why CORR decreases from KTWX-SPR to KTWX-DPR for the May event, we separate our sample size based on the HT and calculate the same statistics presented in Table 3. These statistics are presented in Table 4. We consider the following classes of hydrometeors: rainfall only (RA, HR, BD), hail below the melting layer (HA with RA, HR, and BD), hail above the melting layer (HA, with GR, WS, DS, and IC), and melting layer only (GR, WS, DS, and IC). DPR measurements are better than the SPR measurements for all cases, except when hail is observed above the melting layer, for which the bias increases from 0.56 to 0.84 and the correlation decreases from 0.52 to 0.17. This explains why CORR decreases from KTWX-SPR to KTWX-DPR for the May event, and points out the need to reevaluate the radar rainfall estimation equation for this HT.

d. Time-scale dependency of errors

Radar rainfall errors are expected to decrease with increasing temporal scales because uncertainties that arise from the gauge–radar spatial sampling problem are filtered out. Figure 11 shows how radar rainfall uncertainty changes with temporal scales varying from 15 to 180 min for the March, May, and September events. Based on this figure, radar measurement errors decrease as we aggregate the observations in time. The rate of decrease, however, is different for each event. For the May and September events, CORR does not increase significantly for scales greater than 1 h, while for the March events CORR still increases as we aggregate the observations up to 3 h. SE decreases up to scales of 3 h. As SE is sensitive to the sample size, part of the decrease in SE is caused by the sample size, which decreases as the temporal aggregation increases.

In terms of correlation (CORR), KEAX-DPR exhibits better performance for the March and September events, while KTWX-DPR exhibits slightly better performance for the May event. In terms of standard error (SE), the DPRs provide better performance than the corresponding SPRs for the May and September events. For the March event, KEAX-SPR exhibited the lowest SE among all radar–polarization combinations.

e. Basin-scale analyses of radar rainfall errors

In this section, we investigate how rainfall uncertainties change across different spatial scales delineated by watersheds. We evaluate nested subbasins with drainage area varying from 0.02 to 650 km^2. We use CUENCAS to obtain the river network and basin delineations [see Mantilla and Gupta (2005) for details on the software and the procedure], from the 30-m NED DEM provided by the USGS. All analyses in this section are for the May event.

In Fig. 12, we present correlation and standard error estimates based on the 15-min mean areal rain rate for the May event. We estimate the statistics using as reference 15-min rain gauge rain rates that are spatially interpolated to generate continuous spatial maps. The

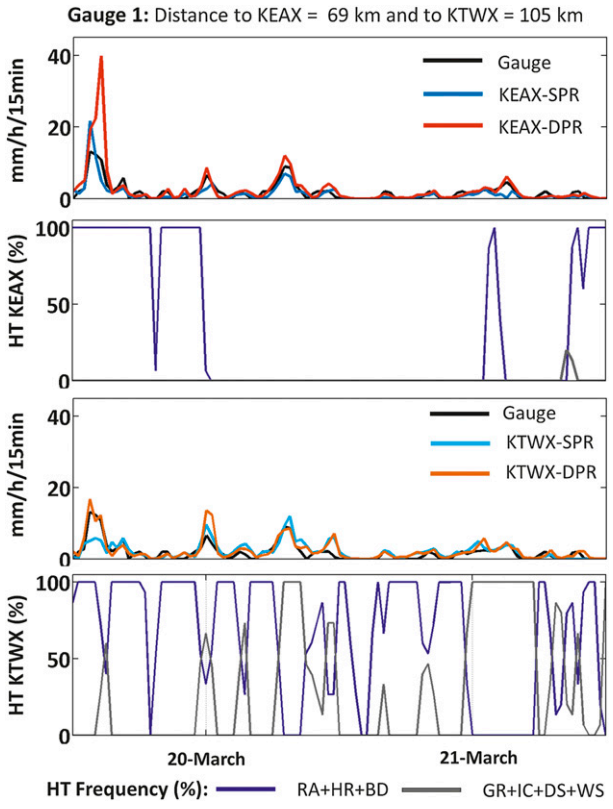

FIG. 8. Rain-rate and HT time series for the March event for gauge 1 located 69 and 105 km from KEAX and KTWX, respectively: (from top to the bottom) the 15-min rain rate based on rain gauge, KEAX-SPR, and KEAX-DPR; HT frequency for rainfall hydrometeors (RA + HR + BD) and HTs typical of the melting layer (GR + IC + DS + WS) for KEAX; and the last two panels, as in the top two, but for KTWX.

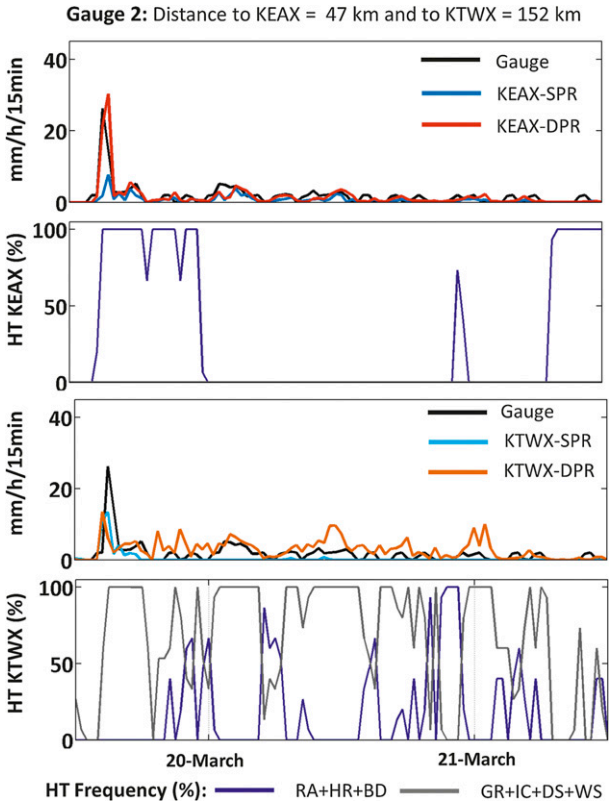

FIG. 9. As in Fig. 8, but for gauge 2 located at 47 and 152 km from KEAX and KTWX, respectively.

red dots represent the values for the KTWX-SPR for the 9357 subbasins. Both statistics present large variability for basins smaller than 1 km^2. This is expected because the radar rainfall data resolution is 1 km^2 and, thus, does not provide accurate information for smaller scales. To remove the effects of random variation and reveal underlying trends, we include moving-average lines for KTWX-SPR (red line) and the remaining radar products. The plots show that correlation increases and standard error decreases with scale for all of the products. DPR products have better statistics than SPR products for the same radar. For the largest drainage area evaluated in this study (650 km^2), CORR is equal to 0.98 and SE to 1.7 mm for the KEAX-DPR, with values of 0.98 and 2.2 mm, respectively, for KTWX-DPR.

In Fig. 13, we present the normalized bias for the mean areal storm total (NB-MAST) for the four radar rainfall products for all nested watersheds. We include regression lines for all plots to assist in the evaluation of the results. The numbers presented in the top-right corner of each plot represent the NB-MAST for the 650 km^2 watershed. NB-MAST equal to 0.0 indicate unbiased data, and values equal to 0.5 (-0.5) mean that the radar overestimated (underestimated) the mean areal storm total by 50%. As the previous analyses demonstrated, KTWX-SPR (KTWX-DPR) has a tendency to underestimate (overestimate) rainfall for the May event. For KTWX-DPR, many of the basins with area smaller than 1 km^2 exhibited NB-MAST values larger than 1, which indicates an overestimation of more than 100%. For the outlet, NB-MAST is equal to -0.26 for KEAX-SPR and 0.66 for KTWX-SPR. Bias decreases for the DPR for both radars, but KTWX-DPR still shows large bias (0.57). This demonstrates the need for more research to improve range-dependent properties of DPR rainfall estimation.

The best product (KEAX-DPR) overestimates the mean areal storm total by 23% at the outlet of the basin (650 km^2). Since rainfall is the major driving force for flood modeling, radar rainfall estimates should be bias corrected before being used as input to flood simulation models. NB-MAST exhibits large variability for basins smaller than 10 km^2 for all products (e.g., -0.8 to 1.0 for KEAX-SPR). In future

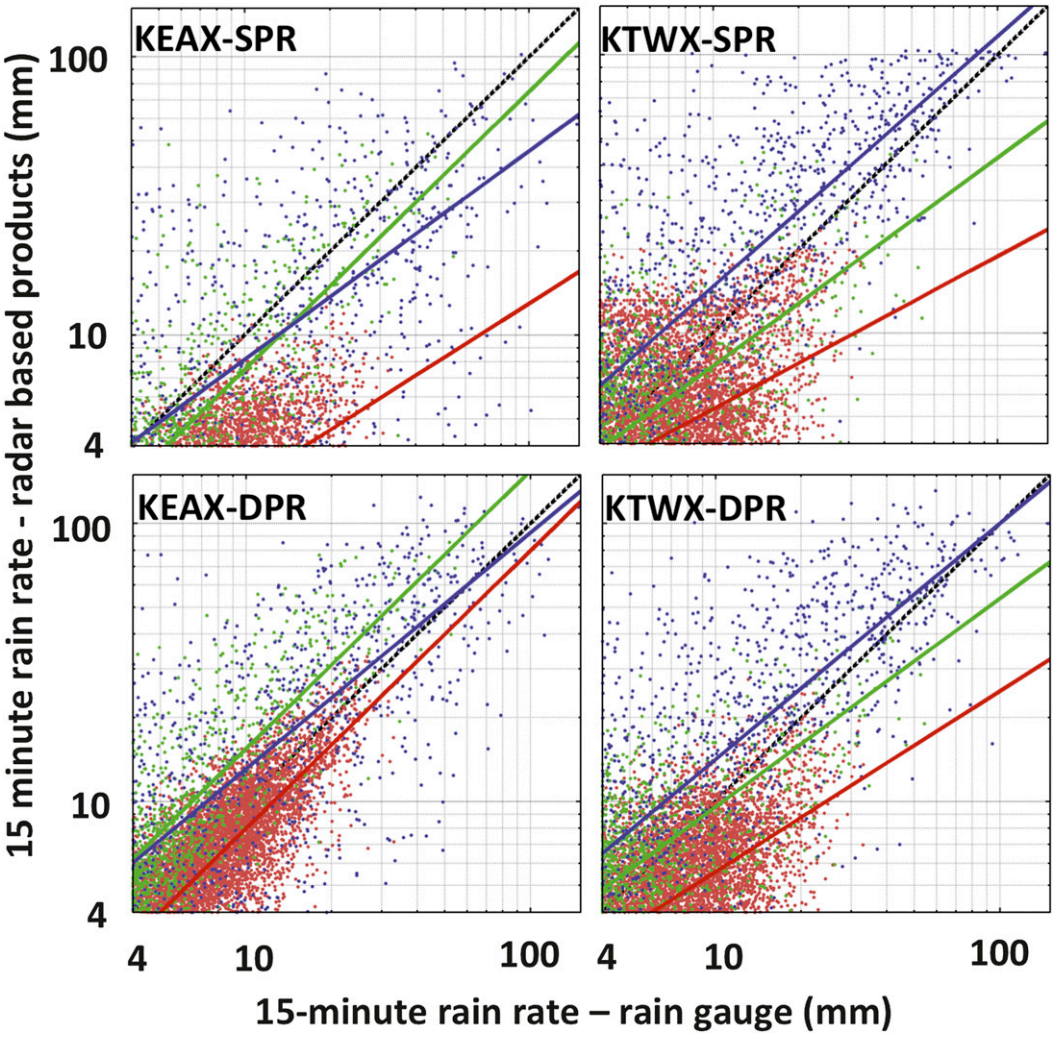

FIG. 10. Gauge–radar scatterplots of 15-min data for (left) KEAX and (right) KTWX with (top) SPR and (bottom) DPR datasets for the March (green), May (blue), and September (red) events. Included are power laws to describe the relationship between rain gauge and radar rain rate for each event.

studies, we will investigate how these uncertainties propagate through hydrologic models and affect their flood predictions.

4. Conclusions

In this study we compare radar rainfall fields based on SPR and DPR measurements from radar. We analyzed rainfall fields developed from the KEAX and KTWX WSR-88Ds, and focus on a 60 km × 60 km study region in Kansas City with a network of 136 rain gauges. The distance from the KEAX radar to rain gauges in the Kansas City network spans from 23 to 72 km, while the distance from the KTWX radar extends from 104 to 157 km. This difference in distance from the radars to the study area allows us to investigate range effects on SPR and DPR rainfall products. Radar rainfall estimates are compared to tipping-bucket rain gauge observations from the dense gauge network in Kansas City. We base our conclusions on analyses of three storm events that occurred in March, May, and September of 2012. The principal conclusions of these analyses are summarized below.

1) For a diverse range of storm types, DPR measurements generally improve the quantitative estimation of rainfall relative to SPR estimates. However, improvements achieved by DPR are not consistent for all events or radars. The nature of the improvement depends fundamentally on range-dependent sampling of the different hydrometeor types.

TABLE 3. The 15-min rain-rate statistics for all rainfall datasets and events.

Event	Dataset	Statistics				No. of time intervals with			
		NB	CORR	SE	Rmax	$R > 0$	$R > 4$	$R > 25$	$R > 100$
Event 1 (No. of sites = 131;	Gauge				54.1	9822	1174	36	0
No. of samples = 201 203)	KEAX-SPR	−0.28	0.68	5.75	52.9	13 880	609	39	0
	KEAX-DPR	0.5	0.82	9.42	85.6	15 646	1780	144	0
	KTWX-SPR	−0.24	0.52	6.44	44.6	10 551	1335	30	0
	KTWX-DPR	−0.02	0.65	5.2	53.5	15 631	3814	30	0
Event 2 (No. of sites = 125;	Gauge				147.5	4000	1078	254	7
No. of samples = 201 205)	KEAX-SPR	−0.35	0.53	18.21	102.1	9399	783	197	1
	KEAX-DPR	0.19	0.68	18.04	124.5	7079	1122	360	11
	KTWX-SPR	0.49	0.72	20.17	103.8	6416	1660	506	13
	KTWX-DPR	0.43	0.69	19.83	131.2	8178	1454	445	16
Event 1 (No. of sites = 132;	Gauge				33.1	12 004	6617	26	0
No. of samples = 201 209)	KEAX-SPR	−0.7	0.45	6.91	13.8	13 553	1117	0	0
	KEAX-DPR	−0.19	0.78	3.19	35.7	14 601	5037	25	0
	KTWX-SPR	−0.43	0.3	5.92	24.9	12 207	4512	0	0
	KTWX-DPR	−0.42	0.46	5.18	29.6	14 732	4114	2	0

2) Improvements in rainfall estimation achieved by the use of DPR measurements are more pronounced for KEAX, the radar located close to the study area. For the far-range KTWX radar, small improvements are observed for the May and September events through the use of DPR measurements. For the March event, rainfall estimates based on the DPR algorithm are better for a range interval of approximately 104–125 km, and worse (overestimation) at a range interval of approximately 125–156 km. This problem is related to the detection of dry snow and ice crystals.
3) For the cases with no brightband contamination or hail, SPR rainfall predictions underestimate the rainfall. This occurs for the March and September events for the KEAX radar, and the September event for the KTWX radar. This is likely the result of using standard parameters for the Z–R relationships that, on average, compensate for some brightband contamination. When mixed-phase hydrometeors are not present, rainfall is underestimated using SPR reflectivity measurements. DPRs are able to detect settings in which rain is observed entirely below the

TABLE 4. The 15-min rain-rate statistics for the May event separated by HHC.

Sample size	Dataset	Statistics				No. of points with			
		NB	CORR	SE	Rmax	$R > 0$	$R > 4$	$R > 25$	$R > 100$
		Just rain (RA, HR, BD)							
3374	Gauge				115.4	2338	830	195	4
	KEAX-SPR	−0.26	0.64	9.39	102.1	3068	573	159	1
	KEAX-DPR	0.29	0.79	9.51	124.4	3374	866	292	7
4176	Gauge				66.6	2105	364	8	0
	KTWX-SPR	0.88	0.6	4.2	91.7	3859	725	40	0
	KTWX-DPR	0.55	0.61	2.78	27.9	4176	589	5	0
		Hail below melting layer (HA with RA, HR, and BD)							
69	Gauge				147.4	69	66	49	3
	KEAX-SPR	−0.5	0.56	33.02	86.9	68	53	24	0
	KEAX-DPR	0.07	0.58	27.21	116.5	69	66	50	4
158	Gauge				147.4	157	148	96	7
	KTWX-SPR	0.66	0.58	36.23	103.8	158	155	138	12
	KTWX-DPR	0.44	0.51	32.63	118.0	158	155	127	12
		Hail above melting layer (HA with GR, WS, DS, and IC)							
37	Gauge				85.9	37	34	15	0
	KTWX-SPR	0.56	0.52	25.18	101.3	37	37	31	1
	KTWX-DPR	0.84	0.17	32.25	88.2	37	37	36	0
		Melting layer (GR, WS, DS, and IC)							
349	Gauge				112.0	252	62	16	1
	KTWX-SPR	0.61	0.8	11.32	103.7	236	128	31	3
	KTWX-DPR	0.68	0.85	9.38	86.8	349	101	36	0

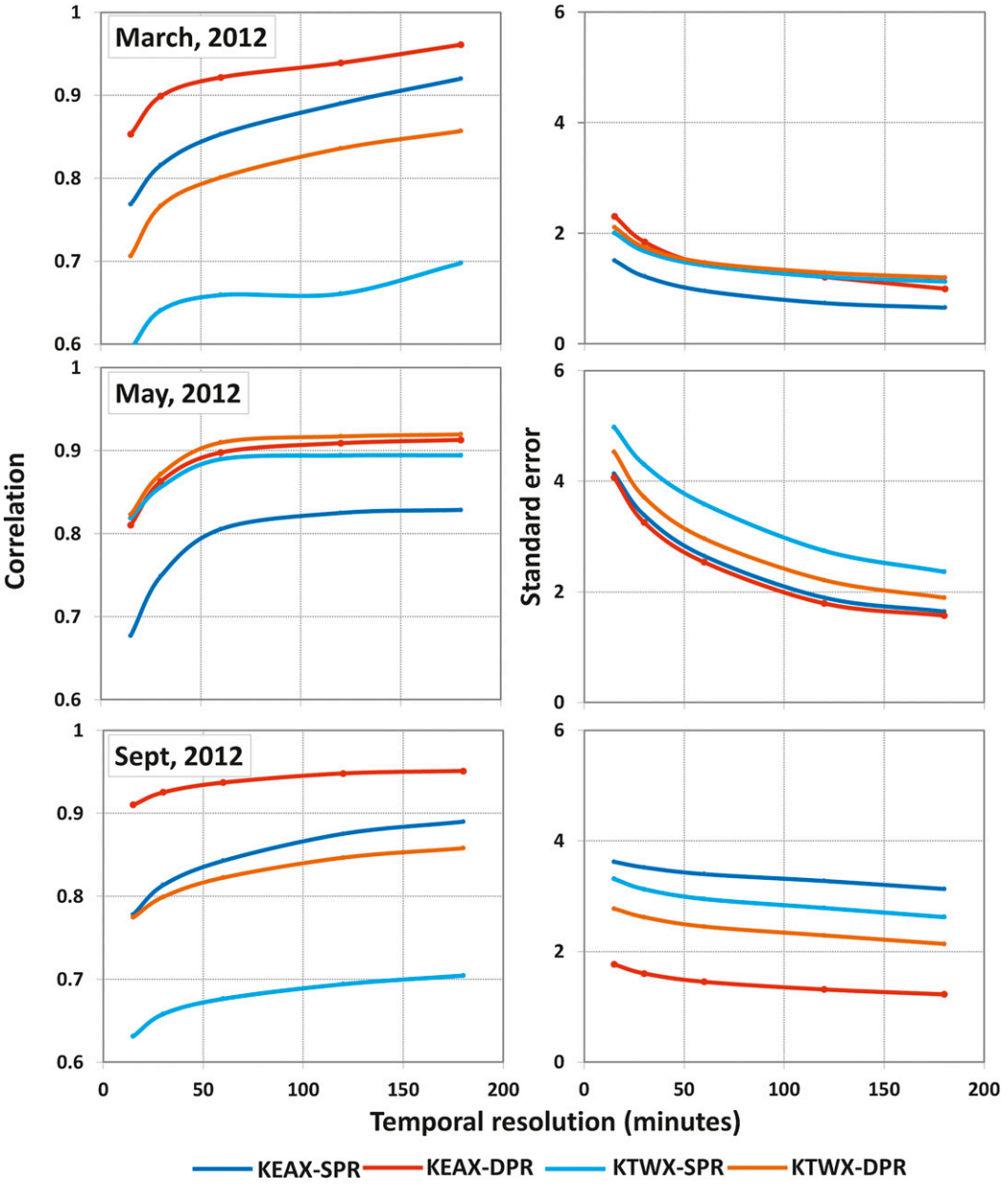

FIG. 11. Error statistics (radar products compared to gauge rainfall data) with respect to temporal scale for (top to bottom) the March, May, and September events: (left) CORR and (right) SE.

bright band. For these situations, rainfall is estimated as a function of reflectivity and differential reflectivity. The addition of differential reflectivity to the rainfall estimation process has a significant positive impact on the values estimated for the KEAX radar.

4) DPRs improved the estimation of rainfall when hail occurred below the top of the melting layer, as was the case for the Kansas City observations during the May event. When hail mixed with rain is detected above the melting layer, as was the case for the KTWX observations of the May storm, we did not find significant improvements from DPR measurements.
5) Radar–rain gauge comparisons demonstrate the large bias for the KEAX-SPR estimates, and the ability of the DPR algorithm to correct this bias. The normalized bias improved from −0.52 to 0.01. KTWX-SPR rain rates are characterized by low bias but large random error, which is slightly improved by the DPR measurements (decrease in standard error from 3.62 to 3.28).

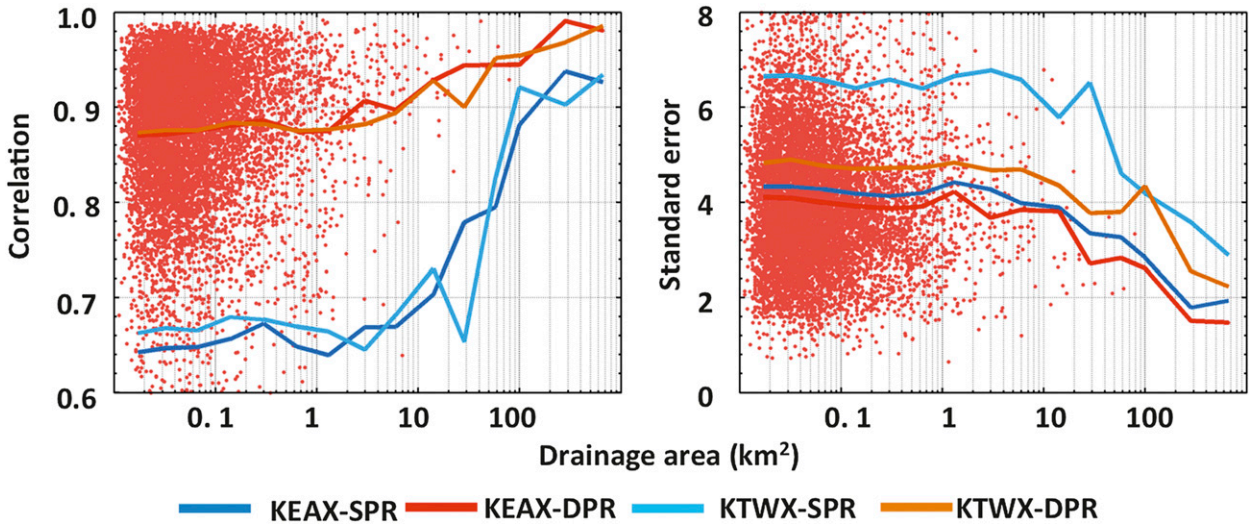

FIG. 12. Error statistics for 15-min rain rates with respect to spatial scale for nested subwatersheds in the study area (May event): (left) CORR and (right) SE.

6) Comparisons of KEAX and KTWX rainfall estimates demonstrate that operational DPR algorithms reduce range effects, relative to SPR rainfall estimates. In general, improvements are substantial when the radar detects only raindrops, but inconsistent otherwise. This might arise from the fact that QPE algorithms were developed based on data collected in Oklahoma during the warm season, when snow is

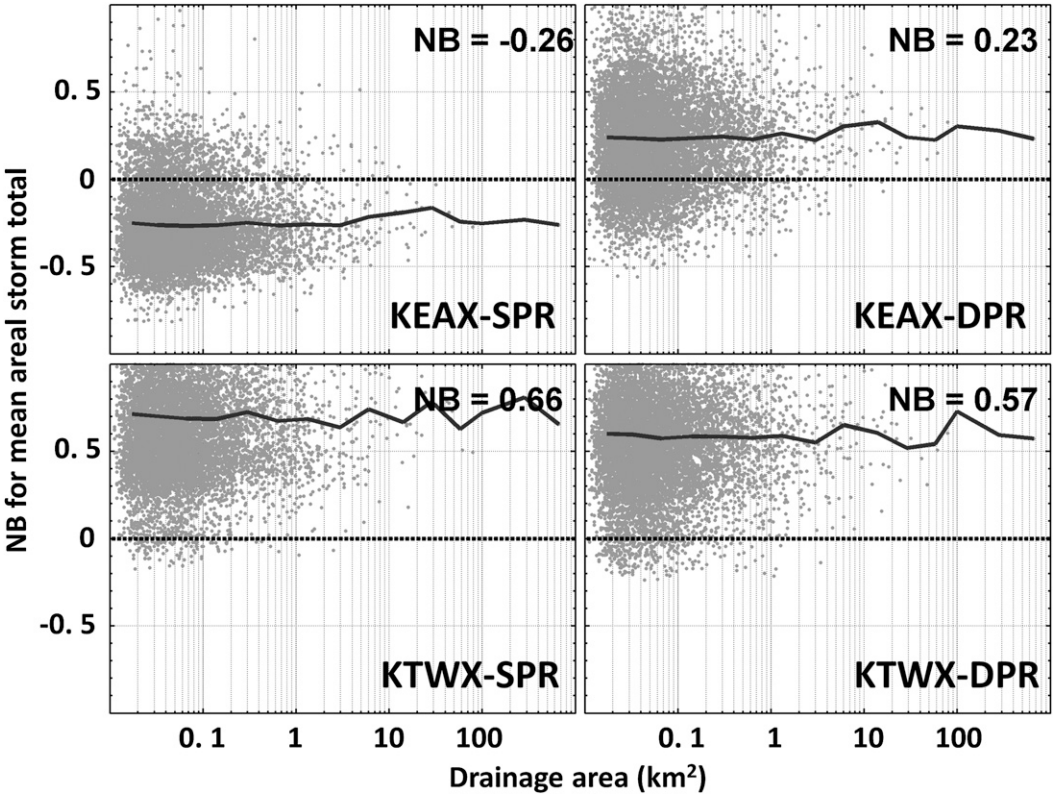

FIG. 13. Mean areal storm total normalized biases as a function of spatial scale for nested subwatersheds in the study area (May event): (top left) KEAX SPR and (top right) DPR; (bottom) as in (top), but for KTWX. The number at the top right of each plot represents the NB for the 650 km^2 watershed.

uncommon in the atmospheric column. Uncertainties in DPR QPEs can also be caused by instrument miscalibration (Ryzhkov et al. 2005a). We cannot further investigate this source of error since we do not have information about the calibration procedures performed in KEAX and KTWX, or long series of data to statistically quantify errors Additional research is needed to address the range-dependent error structure of DPR rainfall estimates.

7) We demonstrate that the error structure of DPR QPEs varies considerably from event to event. This is expected since different radar rainfall algorithms are used depending on the type of hydrometeor observed. Empirical models that characterize rainfall error structure of DPRs (e.g., Villarini et al. 2009) should explicitly account for range-dependent sampling and the effects of HTs.
8) As we aggregate the observations in time, the correlation increases and the standard error decreases for all of the rainfall fields. The correlation did not improve significantly for aggregation times larger than 1 h for the May and September events, while for the March event the correlation continues to increase for aggregation time up to 3 h (maximum aggregation time adopted in the study). For the same radar, DPR rainfall fields provide higher correlations for all events compared to the SPR fields. We also analyze uncertainty as a function of spatial scale. We use basin boundaries to delineate the spatial domain and aggregate the information in space. The analyses demonstrate that for basins up to approximately 20 km^2 the differences in total accumulations obtained by gauges and radar exhibit large variability and reach values of up to 300% for the KTWX-SPR rainfall fields. Differences for larger basins decrease but are still significant. For the largest basin ($\sim$650 km^2) and the best rainfall estimation, storm total radar rainfall is overestimated by 23%. This implies that real-time and retrospective gauge bias correction, as generally applied to SPR, are likely to be useful for DPRs as well.

This paper is an early attempt to evaluate the system recently implemented by the NWS to estimate rainfall based on dual-polarization radars. Future work should include more events, allowing the use of more rigorous statistical approaches to quantify radar rainfall errors as a function of range and hydrometeors types.

Acknowledgments. The authors would like to acknowledge the city of Overland Park Kansas, and specially Mike Ross, for providing helpful comments about the rain gauge network. WFK acknowledges support from the Iowa Flood Center and the Rose and Joseph Summers endowment. This research was supported by the Willis Research Network, the National Science Foundation (Grant CBET-1058027), and the NOAA Cooperative Institute for Climate Science.

REFERENCES

Austin, P. M., 1987: Relation between measured radar reflectivity and surface rainfall. *Mon. Wea. Rev.,* **115,** 1053–1070.

Baeck, M. L., and J. A. Smith, 1998: Estimation of heavy rainfall by the WSR-88D. *Wea. Forecasting,* **13,** 416–436.

Benjamin, S. G., 1989: An isentropic mesoα-scale analysis system and its sensitivity to aircraft and surface observations. *Mon. Wea. Rev.,* **117,** 1586–1603.

Brandes, E. A., and K. Ikeda, 2004: Freezing-level estimation with polarimetric radar. *J. Appl. Meteor.,* **43,** 1541–1553.

Carpenter, T. M., and K. P. Georgakakos, 2004: Impacts of parametric and radar rainfall uncertainty on the ensemble streamflow simulations of a distributed hydrologic model. *J. Hydrol.,* **298,** 202–221, doi:10.1016/j.jhydrol.2004.03.036.

Chandrasekar, V., V. N. Bringi, N. Balakrishnan, and D. S. Zrnić, 1990: Error structure of multiparameter radar and surface measurements of rainfall. Part III: Specific differential phase. *J. Atmos. Oceanic Technol.,* **7,** 621–629.

Ciach, G. J., 2003: Local random errors in tipping-bucket rain gauge measurements. *J. Atmos. Oceanic Technol.,* **20,** 752–759.

——, and W. F. Krajewski, 1999: On the estimation of radar rainfall error variance. *Adv. Water Resour.,* **22,** 585–595, doi:10.1016/S0309-1708(98)00043-8.

——, ——, and G. Villarini, 2007: Product-error-driven uncertainty model for probabilistic quantitative precipitation estimation with NEXRAD data. *J. Hydrometeor.,* **8,** 1325–1347.

Cunha, L. K., W. F. Krajewski, and R. Mantilla, 2011: A framework for flood risk assessment under nonstationary conditions or in the absence of historical data. *J. Flood Risk Manage.,* **4,** 3–22.

——, P. V. Mandapaka, W. F. Krajewski, R. Mantilla, and A. A. Bradley, 2012: Impact of radar-rainfall error structure on estimated flood magnitude across scales: An investigation based on a parsimonious distributed hydrological model. *Water Resour. Res.,* **48,** W10515, doi:10.1029/2012WR012138.

Einfalt, T., K. Arnbjerg-Nielsen, C. Golz, N.-E. Jensen, M. Quirmbach, G. Vaes, and B. Vieux, 2004: Towards a roadmap for use of radar rainfall data in urban drainage. *J. Hydrol.,* **299,** 186–202.

Fabry, F., G. L. Austin, and D. Tees, 1992: The accuracy of rainfall estimates by radar as a function of range. *Quart. J. Roy. Meteor. Soc.,* **118,** 435–453.

Fo, A. J. P., K. C. Crawford, and C. L. Hartzell, 1998: Improving WSR-88D hourly rainfall estimates. *Wea. Forecasting,* **13,** 1016–1028.

Fulton, R. A., J. P. Breidenbach, D.-J. Seo, D. A. Miller, and T. O'Bannon, 1998: The WSR-88D rainfall algorithm. *Wea. Forecasting,* **13,** 377–395.

Germann, U., G. Galli, M. Boscacci, and M. Bolliger, 2006: Radar precipitation measurement in a mountainous region. *Quart. J. Roy. Meteor. Soc.,* **132,** 1669–1692.

Gesch, D., G. Evans, J. Mauck, J. Hutchinson, and W. J. Carswell Jr., 2009. *The National Map*—Elevation. U.S. Geological Survey Fact Sheet 2009-3053, 4 pp. [Available online at http://pubs.usgs.gov/fs/2009/3053/.]

Giangrande, S. E., and A. V. Ryzhkov, 2008: Estimation of rainfall based on the results of polarimetric echo classification. *J. Appl. Meteor. Climatol.,* **47,** 2445–2460.

——, J. M. Krause, and A. Ryzhkov, 2008: Automatic designation of the melting layer with a polarimetric prototype of the WSR-88D radar. *J. Appl. Meteor. Climatol.,* **47,** 1354–1364.

Habib, E., W. F. Krajewski, and A. Kruger, 2001: Sampling errors of tipping-bucket rain gauge measurements. *J. Hydrol. Eng.,* **6,** 159–166.

Heinselman, P. L., and A. V. Ryzhkov, 2006: Validation of polarimetric hail detection. *Wea. Forecasting,* **21,** 839–850.

Istok, M. J., M. Fresch, Z. Jing, and S. Smith, 2009: WSR-88D dual polarization initial operational capabilities. Preprints, *25th Conf. on International Interactive Information and Processing Systems (IIPS) for Meteorology, Oceanography, and Hydrology,* Phoenix, AZ, Amer. Meteor. Soc., 15.5. [Available online at https://ams.confex.com/ams/pdfpapers/148927.pdf.]

Javier, J. R. N., J. A. Smith, K. L. Meierdiercks, M. L. Baeck, and A. J. Miller, 2007: Flash flood forecasting for small urban watersheds in the Baltimore metropolitan region. *Wea. Forecasting,* **22,** 1331–1344.

Knox, R., and E. N. Anagnostou, 2009: Scale interactions in radar rainfall estimation uncertainty. *J. Hydrol. Eng.,* **14,** 944–953.

Krajewski, W. F., and J. A. Smith, 2002: Radar hydrology: Rainfall estimation. *Adv. Water Resour.,* **25,** 1387–1394, doi:10.1016/S0309-1708(02)00062-3.

——, B.-C. Seo, A. Kruger, P. Domaszczynski, G. Villarini, and C. Gunyon, 2007: Hydro-NEXRAD radar-rainfall estimation algorithm development, testing and evaluation. *Proc. World Environmental and Water Resources Congress 2007: Restoring Our Natural Habitat,* Reston, VA, American Society of Civil Engineers, 9 pp., doi:10.1061/40927(243)279.

——, A. Kruger, J. A. Smith, R. Lawrence, and C. Gunyon, 2011a: Towards better utilization of NEXRAD data in hydrology: An overview of Hydro-NEXRAD. *J. Hydroinf.,* **13,** 255–266.

——, B. Vignal, B.-C. Seo, and G. Villarini, 2011b: Statistical model of the range-dependent error in radar-rainfall estimates due to the vertical profile of reflectivity. *J. Hydrol.,* **402,** 306–316, doi:10.1016/j.jhydrol.2011.03.024.

Lanza, L. G., and L. Stagi, 2008: Certified accuracy of rainfall data as a standard requirement in scientific investigations. *Adv. Geosci.,* **16,** 43–48.

Mandapaka, P. V., W. F. Krajewski, G. J. Ciach, G. Villarini, and J. A. Smith, 2009: Estimation of radar-rainfall error spatial correlation. *Adv. Water Resour.,* **32,** 1020–1030, doi:10.1016/j.advwatres.2008.08.014.

Mantilla, R., and V. K. Gupta, 2005: A GIS numerical framework to study the process basis of scaling statistics on river networks. *IEEE Geophys. Remote Sens. Lett.,* **2,** 404–408.

Park, H. S., A. V. Ryzhkov, and D. S. Zrnić, 2009: The hydrometeor classification algorithm for the polarimetric WSR-88D: Description and application to an MCS. *Wea. Forecasting,* **24,** 730–748.

Reed, S. M., and D. R. Maidment, 1999: Coordinate transformations for using NEXRAD data in GIS-based hydrologic modeling. *J. Hydrol. Eng.,* **4,** 174–182.

Ryzhkov, A. V., S. E. Giangrande, V. M. Melnikov, and T. J. Schuur, 2005a: Calibration issues of dual-polarization radar measurements. *J. Atmos. Oceanic Technol.,* **22,** 1138–1155.

——, ——, and T. J. Schuur, 2005b: Rainfall estimation with a polarimetric prototype of WSR-88D. *J. Appl. Meteor.,* **44,** 502–515.

Schröter, K., X. Llort, C. Velasco-Forero, M. Ostrowski, and D. Sempere-Torres, 2011: Implications of radar rainfall estimates uncertainty on distributed hydrological model predictions. *Atmos. Res.,* **100,** 237–245.

Schuur, T. J., H.-S. Park, A. V. Ryzhkov, and H. D. Reeves, 2011: Classification of precipitation types during transitional winter weather using the RUC model and polarimetric radar retrievals. *J. Appl. Meteor. Climatol.,* **51,** 763–779.

Seo, B.-C., and W. F. Krajewski, 2010: Scale dependence of radar rainfall uncertainty: Initial evaluation of NEXRAD's new super-resolution data for hydrologic applications. *J. Hydrometeor.,* **11,** 1191–1198.

——, and ——, 2011: Investigation of the scale-dependent variability of radar-rainfall and rain gauge error correlation. *Adv. Water Resour.,* **34,** 152–163, doi:10.1016/j.advwatres.2010.10.

——, L. K. Cunha, and W. F. Krajewski, 2013: Uncertainty in radar-rainfall composite and its impact on hydrologic prediction for the eastern Iowa flood of 2008. *Water Resour. Res.,* **49,** 2747–2764, doi:10.1002/wrcr.20244.

Smith, J. A., D.-J. Seo, M. L. Baeck, and M. D. Hudlow, 1996: An intercomparison study of NEXRAD precipitation estimates. *Water Resour. Res.,* **32,** 2035–2045.

——, M. L. Baeck, J. E. Morrison, P. L. Sturdevant-Rees, D. F. Turner-Gillespie, and P. D. Bates, 2002: The regional hydrology of extreme floods in an urbanizing drainage basin. *J. Hydrometeor.,* **3,** 267–282.

——, ——, K. L. Meierdiercks, A. J. Miller, and W. F. Krajewski, 2007: Radar rainfall estimation for flash flood forecasting in small urban watersheds. *Adv. Water Resour.,* **30,** 2087–2097.

Steiner, M., and J. A. Smith, 2002: Use of three-dimensional reflectivity structure for automated detection and removal of nonprecipitating echoes in radar data. *J. Atmos. Oceanic Technol.,* **19,** 673–685.

Straka, J. M., D. S. Zrnić, and A. V. Ryzhkov, 2000: Bulk hydrometeor classification and quantification using polarimetric radar data: Synthesis of relations. *J. Appl. Meteor.,* **39,** 1341–1372.

Szturc, J., K. Ośródka, A. Jurczyk, and L. Jelonek, 2008: Concept of dealing with uncertainty in radar-based data for hydrological purpose. *Nat. Hazards Earth Syst. Sci.,* **8,** 267–279.

Villarini, G., and W. F. Krajewski, 2009: Review of the different sources of uncertainty in single polarization radar-based estimates of rainfall. *Surv. Geophys.,* **31,** 107–129.

——, ——, G. J. Ciach, and D. L. Zimmerman, 2009: Product-error-driven generator of probable rainfall conditioned on WSR-88D precipitation estimates. *Water Resour. Res.,* **45,** W01404, doi:10.1029/2008WR006946.

Vulpiani, G., and S. Giangrande, 2009: Rainfall estimation from polarimetric S-band radar measurements: Validation of a neural network approach. *J. Appl. Meteor. Climatol.,* **48,** 2022–2036.

Wilson, J. W., and E. A. Brandes, 1979: Radar measurement of rainfall—A summary. *Bull. Amer. Meteor. Soc.,* **60,** 1048–1058.

Wright, D. B., J. A. Smith, G. Villarini, and M. L. Baeck, 2012: The hydroclimatology of flash flooding in Atlanta. *Water Resour. Res.,* **48,** W04524, doi:10.1029/2011WR011371.

Zawadzki, I. I., 1975: On radar-raingage comparison. *J. Appl. Meteor.,* **14,** 1430–1436.